Equatorial Velocity Profiles. Part II: Zonal Component

KATHLEEN O'NEILL[1]

National Center for Atmospheric Research,[2] Boulder, CO 80307

JAMES R. LUYTEN

Woods Hole Oceanographic Institution, Woods Hole, MA 02543

(Manuscript received 14 November 1983, in final form 22 September 1984)

ABSTRACT

Vertical profiles of horizontal velocity made along 53°E in the western Indian Ocean, during and after the onset of the southwest monsoon in 1976, show features in zonal velocity of relatively small vertical scale. Persistence of the features over the month-long observation period and over 2½ degrees of longitude indicates long temporal and zonal scales. The vertical structure is common to those profiles close to the equator, with no appreciable variation in amplitude or depth. Between 1°30′N and 3°N the phase of the features reverses. There is no evidence of similar features at 5°N.

The data suggest meridionally trapped equatorial waves. Similarities between the observed phenomena and the linear theory of equatorial waves are striking but quantitative comparisons lead us to question its naïve application here. Equatorial intensification is apparent but it does not scale with the Rossby radius of deformation, indicating that Kelvin waves are not dominant at any vertical scale. The phase change and corresponding amplitudes of zonal velocity do not fit a low-frequency, first meridional-mode long Rossby wave. Higher meridional modes produce further inconsistencies. There is no evidence of vertical propagation of the larger scale features.

Although the small vertical scale variability is ubiquitous in the equatorial regions, no satisfactory theory exists at present. Our conclusion is that although there are similarities between observations and linear theory, there are serious discrepancies which may be related to the proximity of these observations to the slanting coast of East Africa.

1. Introduction

A section of vertical profiles of horizontal velocity was occupied in 1976 along 53°E, extending from 0°45′S to 5°N, in the western Indian Ocean. The section was repeated several times over a month, during the onset of the southwest monsoon. The zonal velocity profiles show features whose vertical scale is a fraction of the ocean depth, which persist through the duration of the observations.

The zonal component of the velocity profiles appears to be quite different from the meridional component, as discussed in O'Neill (1984; hereinafter referred to as Part I). Time scales and both vertical and horizontal length scales are longer for the zonal component. The separation in time scales between zonal and meridional components is characteristic of equatorial currents in general (Luyten, 1982; Luyten and Roemmich, 1982; Weisberg and Horigan, 1981).

The time scale indicated by the zonal profiles is significantly longer than the duration of the measurements. The equatorial features described in Luyten and Swallow (1976) persist over the month-long observation period not only at the equator but off the equator as far as 3°N. They are in phase with the equator through 1°30′N, and the phase at 3°N is reversed by comparison. The vertical scale of the features increases as one moves away from the equator and there is no evidence of vertical propagation.

Such small vertical scale features are found at midlatitudes, where they are associated with near-inertial waves (Sanford, 1975). Prior to the measurements reported here, there had been several observations of small vertical scale velocity structure in the equatorial oceans. However, these observations spanned only short intervals so that it is not possible to estimate time scales. In the mid-Pacific, Taft *et al.* (1974) lowered a current meter to 1000 m at the equator and at 1°N and to 2000 m at 1°S, 150°W, providing evidence of strong westward flows beneath the undercurrent with vertical scales of 100–200 m and amplitudes of up to 40 cm s^{-1}. The flow at 1°S is similar to that at the equator, and in the additional 1000 m of data at 1°S, the flow reverses twice more. In the western Pacific, Rual's (1969) observations

[1] Present affiliation: Ocean Climate Research Division, NOAA/PMEL, Seattle, Washington 98115.

[2] The National Center for Atmosphere Research is sponsored by the National Science Foundation.

between 1000 and 1500 m at 170°E show westward flows with a vertical scale of 300 m within 1° of the equator, with predominantly eastward flows on either side. Perhaps the first strong evidence of complex vertical structure is from Soviet latitudinal and zonal transects to a depth of 1000 m in the western Pacific Ocean, showing three to four flow reversals in that depth interval (Kort *et al.*, 1966).

Because of space constraints, not all of the 1976 profile data is presented here. However, the full set of forty velocity profiles is available in Spencer *et al.* (1980), along with details of data quality and processing. Further information on procedures applied to the data can be found in O'Neill (1982), where the complete set of latitudinal and temporal sections in both original and WKB-scaled form are contained in Appendices A and B.

In Section 2, the original and WKB-scaled data are described, and comparisons are made with other observations. In Section 3, spectral analysis results are presented, followed by interpretation and discussion in Section 4. Section 5 contains further discussion and conclusions.

2. Data

a. Zonal velocity

The velocity profiles were obtained using an acoustic dropsonde, the White Horse. Details of the data processing are described in Part I. The time series of zonal velocity profiles at 0°, 53°E is shown in Fig. 1a. Similarities between the profiles are striking. Many features of the profile from 16 May 1976 are evident in the profile from 17 June, particularly in the upper 2000 m. The same is true at 0°45′N, as can be seen in the time series from that location shown in Fig. 1b.

Figure 1c is from the third (of eight) latitudinal transect along 53°E, spanning 2–5 June 1976. All six transects which included 3°N show the same features: strong similarity between the profiles at and near the equator, with a broadening in the vertical of the features away from the equator along with the absence at 1°30′N of some features common to the equator and ±0°45′; and at 3°N, some of the same features, but reversed in phase, with flow in the opposite direction. The profiles at 5°N, by contrast, show a much longer vertical scale with little vertical structure.

Westward flow defines the majority of the features at the equator, with amplitudes at times greater than 50 cm s^{-1} at 200 m, amplitudes of up to 40 cm s^{-1} at 700–750 m, and amplitudes of 10–20 cm s^{-1} at 1200 m and at 2000 m. The uppermost jet is observed at ±0°45′ and, during the later part of the time series, at 1°30′N. The jet at 700–750 m is observed throughout the time series through 1°30′N, as is eastward flow at the same depth at 3°N. The westward flow at 1200 m is observed only at the equator and 0°45′N for the duration of the observations. Westward flow at 2000 m is observed at near-equatorial stations throughout the time series, corresponding to eastward flow at 3°N. The vertical scale of the features increases with depth at all profile stations.

b. Vertical displacement

Profiles of the vertical displacement of isopycnal surfaces from a reference surface were calculated from the White Horse CTD data by subtracting a space–time average of potential density (computed using all CTD data between 0°45′S and 3°N, 53°E) from each potential density profile and dividing locally by the mean potential density gradient. Although there may be consistent horizontal variations in the temporal mean density field, our data cannot determine them and so we have chosen to ignore them for the present discussion. The underlying assumption is that spatial averaging over four degrees of latitude and temporal averaging over three weeks provides a sufficient approximation to the equilibrium density field.

The temporal and latitudinal sections of vertical displacement corresponding to the zonal velocity sections of Fig. 1 are shown in Fig. 2. For this latitudinal section, the CTD data at the equator were incomplete.

c. WKB stretching and normalizing

Inspection of the profiles shown in Fig. 1 reveals that, although the vertical structure is consistent, the scale increases with increasing depth. In order to obtain more vertically homogeneous data, we apply a WKB-scaling procedure to both the zonal velocity and the vertical displacement profiles. The scaling for zonal velocity, vertical displacement and the vertical coordinate are

$$\left.\begin{aligned} u^* &= [N_0/\bar{N}(z)]^{1/2}u \\ \zeta^* &= [\bar{N}(z)/N_0]^{1/2}\zeta \\ z^* &= \int \frac{\bar{N}(z)}{N_0}\,dz \end{aligned}\right\}.$$

The background and details are given in Part I. This scaling accounts for the expected structure in the fields due to depth variations in the mean static stability.

The stretched and scaled velocity fields, shown in Fig. 3, show the same features as the raw data except that the amplitudes and vertical scales are more uniform. In particular, these scaled profiles show that variability at a vertical stretched wavelength of approximately 1500 stretched meters (sm) extends from the equator out to 3°N (see Fig. 3b). The shorter vertical scales are more strongly confined to the equator. The scaled vertical displacement profiles in

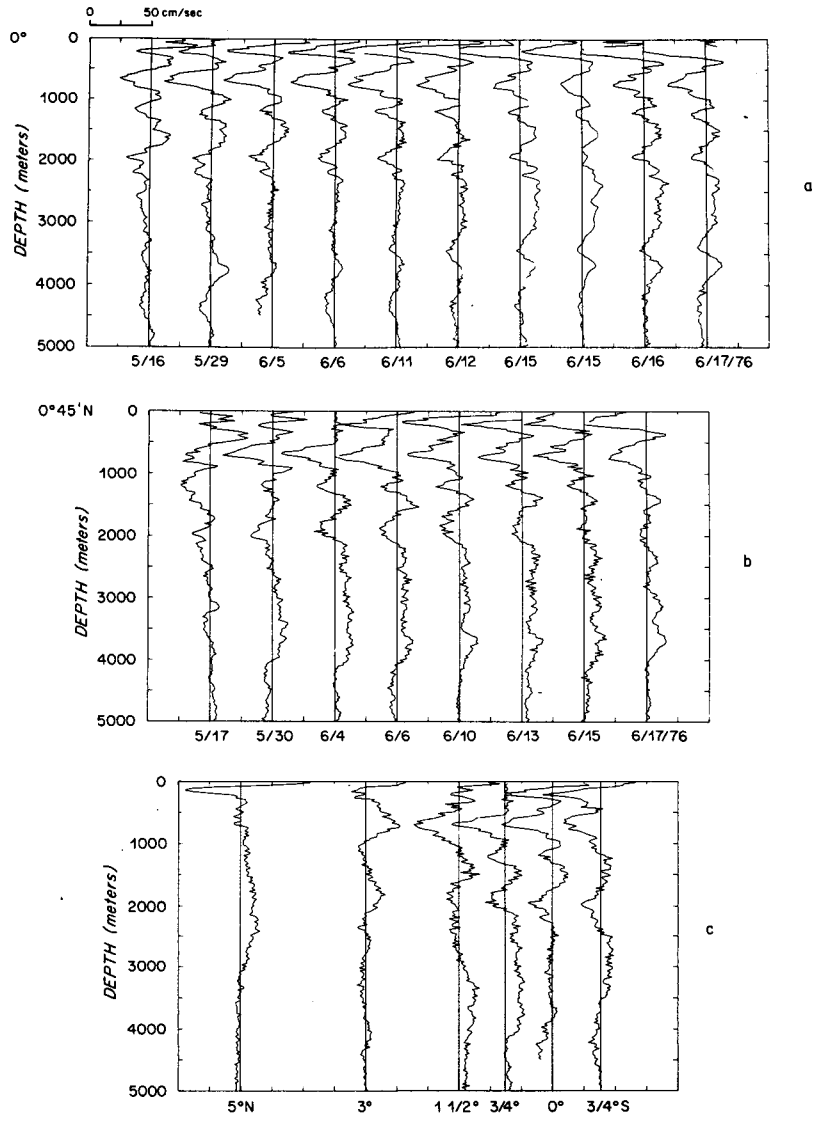

FIG. 1. (a) Time series of zonal velocity profiles from 0°, 53°E spanning 16 May–17 June 1976; (b) time series of same from 0°45′N, 53°E spanning 17 May–17 June; (c) latitudinal section of zonal velocity from a transect along 53°E from 0°45′S to 5°N.

Fig. 4, however, exhibit neither the persistence with time nor latitude evident for zonal velocity.

d. Comparison with other observations

The persistence with time of small-scale vertical structure at the equator can be compared with results from the western Pacific and from the eastern Pacific. At 179°E there are strong similarities between profiles of both east velocity and vertical displacement taken over a time span of six days (Eriksen, 1981). At 110°W Hayes (1981) finds stronger similarities over a period of 2.3 days for north velocity (especially when plotted on constant potential density surfaces, viz. his Fig. 15) and vertical displacement profiles than for east velocity profiles. Eriksen's (1981) latitudinal sections at 179 and 168°E indicate some features common to the equator and 0° ± 45′, but no similarity at ±1°30′ and, in particular, no counterpart to the phase reversal we find along 53°E between 1°30′N and 3°N. Our east velocity and displacement profiles bear no obvious relationship to each other, in contrast with Eriksen's (1981) results at 0°, 179°E.

There are similar indications of the latitudinal structure of zonal velocity seen here in the observations of Tsuchiya (1975), Cochrane *et al.* (1979), and Molinari (1982) of subthermocline undercurrents in the Pacific and Atlantic Oceans. Eastward flows appear to be symmetric about the equator at latitudes between

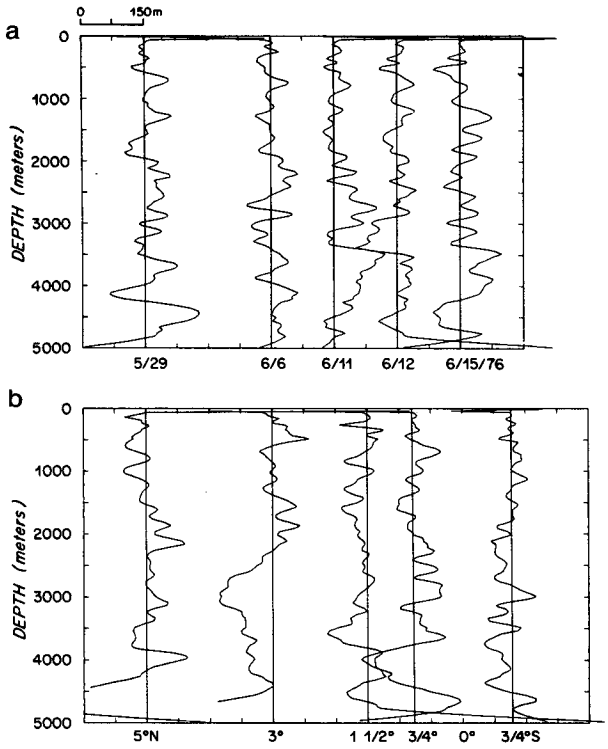

FIG. 2. (a) Time series of vertical displacement profiles from 0°, 53°E; (b) latitudinal section of vertical displacement from same transect as Fig. 1c.

3 and 6° from the equator. These undercurrents are in general surrounded by westward flow and are usually distinct from the shallower equatorial undercurrent, although sometimes appearing as downward extensions of it (Hisard *et al.*, 1970). In all cases, these undercurrents appear to be permanent features of the near-equatorial flow field. The observations are in the upper 800 m, and no information about deeper reversals is available.

The permanence of the latitudinal structure in the western Indian Ocean can be examined by reference to other profile observations from 1979 (Levy *et al.*, 1982) and current meter observations from 1976 (Luyten, 1982) and 1979–80 (Luyten and Roemmich, 1982). In 1976 there were current meters at only one of the depths where jets are observed in the profiles, 200 m at both 53 and 50°30'E on the equator. These records indicate a breakdown in the westward flow at that depth in late July, followed by periods of energetic, but variable in direction, flow for the remainder of the 8-month duration of the experiment. The 1979–80 current meter data for depths of 200, 500 and 750 m along the equator from 47 to 62°E, with records 45' off the equator at 51 and 59°E, span 14 months. The strongest signal in zonal velocity is at a semiannual period. The phase of the observed semiannual cycle is such that there is westward flow at all locations at 750 m during May through early July 1979.

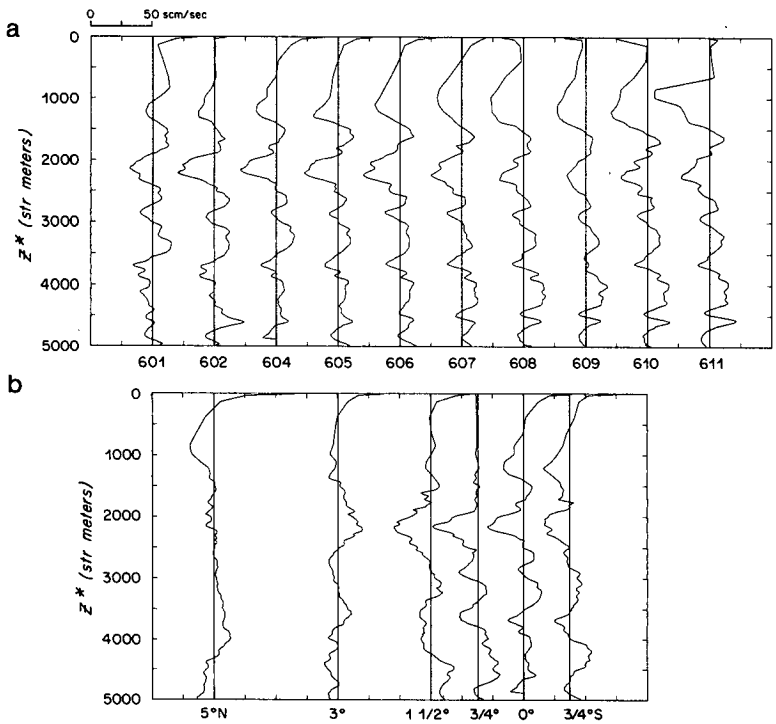

FIG. 3. WKB-scaled zonal velocity profiles: (a) same time series as Fig. 1a; (b) same latitudinal section as Fig. 1c.

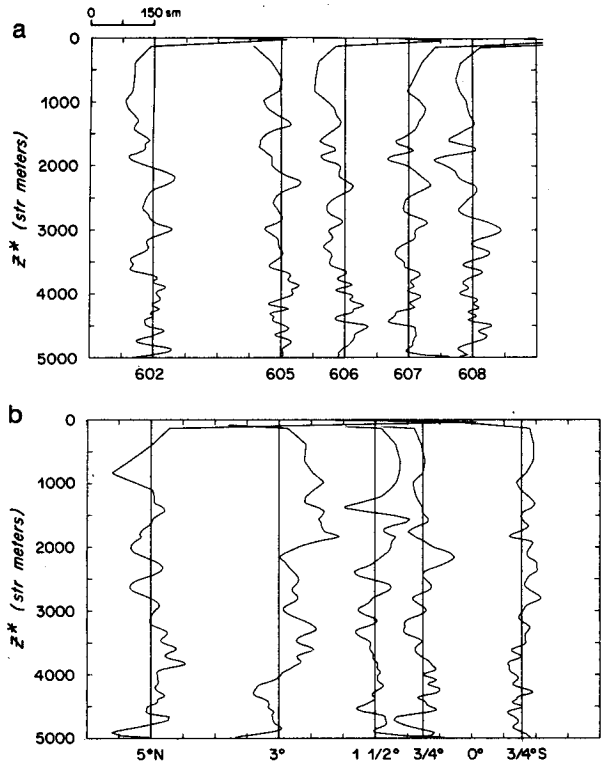

FIG. 4. WKB-scaled vertical displacement profiles: (a) same time series as Fig. 2a; (b) same latitudinal section as Fig. 2b.

The latitudinal sections of White Horse profiles in 1979 are at 51°E, two degrees west of the 1976 profile sections. Meridional spacing was 0°, −0°45′, ±2° and ±4° for the 4–8 April transect and 0°, ±0°45′ for the 24–26 June transect (Levy *et al.*, 1982). The near-equatorial profiles in April show westward flow in the upper 3000 m, with short vertical scale westward features superimposed. The shorter scale features, with amplitudes up to 20 cm s^{-1} above the background flow, appear at the equator at depths of 250, 600, 900, 1100, 1500 and 2000 m. Flow at 2°N is eastward from 250 to 2000 m, with eastward features at 400 and 600 m. The flow at 2°S does not appear to be even weakly related to that at the equator. Flow at ±4° exhibits very long vertical scales.

The June 1979 section, with severely abbreviated latitudinal extent, is quite different from that two and a half months earlier. Flow is westward only in the upper 1500 m of these profiles. There are westward jets at 250, 600, 1300 and 1800 m, with the latter only apparent at the equator and 0°45′S. Both sections appear to be dominated by a combination of longer and shorter vertical scales than the 1976 data. While it is possible that an existing latitudinal structure was simply not resolved by the 1979 station spacing, there is no evidence that the dominant features at and near the equator reverse with higher latitude in 1979.

3. Analysis

a. Autospectra

The autospectrum of the variance of zonal velocity is computed with respect to stretched vertical wavenumber. A variance-preserving plot of this spectrum at each profiling station along 53°E is presented in Fig. 5. Each curve is for a particular latitude, and no averaging over wavenumber bands was performed. The estimates for the equator are averages for ten profiles; at 0°45′S and 5°N for only three. Only the bottom 3600 sm of the WKB-scaled profiles were used in the computation of spectral plots, for reasons discussed in Part I.

The strongest single signal is the peak for a wavelength of 720 sm, which at the equator and 0°45′S is significant at the 95% confidence level. A secondary peak appears only at these two profiling stations for a wavelength of 360 sm, also significant.

Because the common vertical scale appears to be close to 1500 sm (from Fig. 3), which falls between the bands centered at 1800 sm and 1200 sm which are resolvable when the series length used is 3600 sm, that series was decremented at the top and bottom to 3200 sm in order to examine the effects of variations in the discretization of vertical wavelength

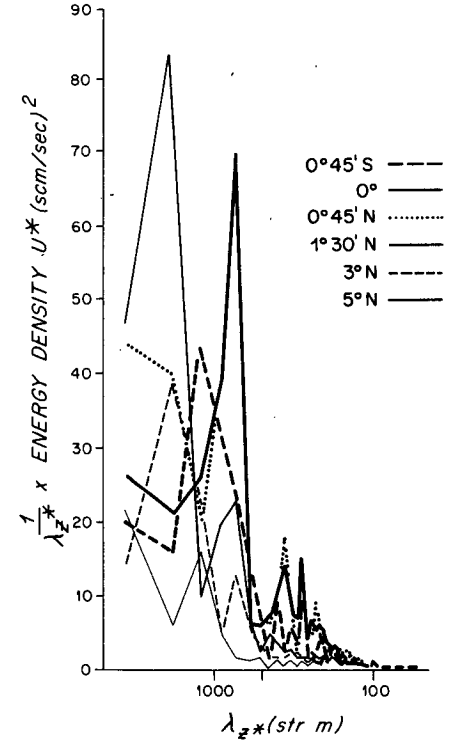

FIG. 5. Variance-preserving autospectra of WKB-scaled zonal velocity, presented for each profiling station along 53°E as a function of stretched vertical wavenumber. Spectra computed by piece-averaging periodograms for each station, with no wavenumber averaging.

bands. The major differences in the autospectra at 0° and 0°45'N are a drop in zonal kinetic energy at a vertical wavelength of 1067 sm, relative to 1200 sm, and an increase at 1600 sm, relative to 1200 and 1800 sm. At both latitudes the trough in zonal kinetic energy at a vertical wavelength of 1067 sm is statistically significant at the 95% confidence level.

b. Spectral energy distribution with latitude

The latitudinal distribution of zonal kinetic energy as a function of vertical wavenumber is shown in Fig. 6. Each point plotted represents an average over five adjacent wavenumber bands. An intensification of energy near the equator is evident in the higher wavenumber bands and is particularly strong for 240 sm. The energy density estimates are significantly different from each other at the equator and 1°30'N for all four wavenumber bands. The estimates for the 720 and the 360 sm bands are separated by an order of magnitude at each latitude.

Comparison with the corresponding figure for north velocity (Fig. 6, Part I) indicates that only the low-order estimates are significantly different at any latitude, with zonal kinetic energy higher than meridional. These estimates can also be compared with the latitudinal distribution of energy reported at 179°E by

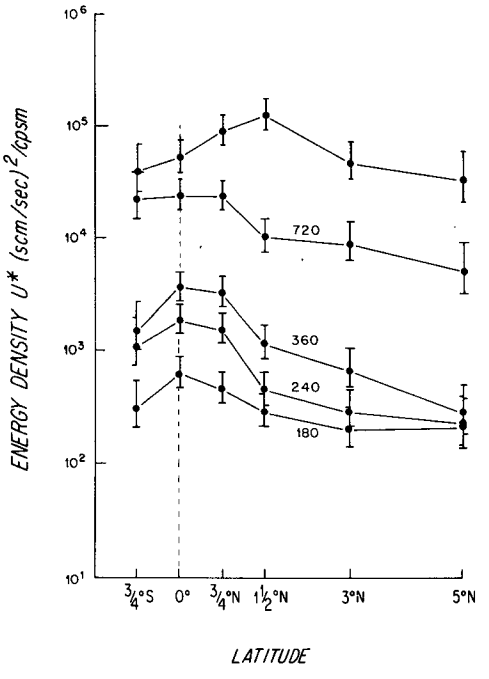

FIG. 6. Autospectra of WKB-scaled zonal velocity, piece-averaged and averaged over five wavenumber bands at each station, presented as a function of latitude from 0°45'S to 5°N. The lower four curves are labeled by the center wavelength (in stretched meters) of the averaging interval. The unlabeled curve at the top of the figure is the low-order estimate. Error bars represent 95% confidence interval limits.

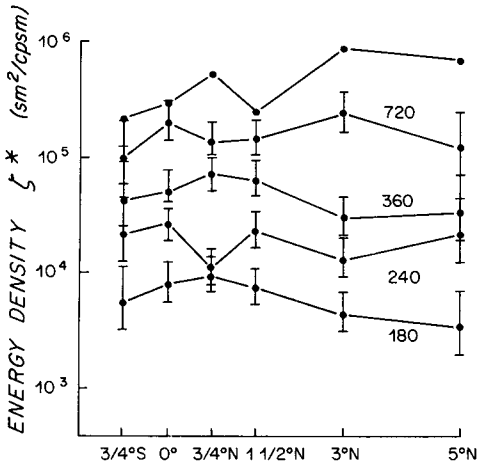

FIG. 7. As in Fig. 6 but for vertical displacement.

Eriksen (1981). The averaging intervals used here and by Eriksen are equivalent, e.g., 720 sm directly corresponds to his 800 sdb, since the reference buoyancy frequencies used are 1.09 and 1 cph, respectively. Although the zonal kinetic energy at 720 sm (800 sdb) is comparable at the equatorial sites, we find significantly (at the 95% confidence level) more energy at 0°45'N and 3°N than Eriksen (1981) finds in the western Pacific. There are no other significant differences.

Figure 7 shows the similarly averaged autospectral estimates by latitude for the vertical displacement field. Except for the dip at 0°45'N for a wavelength of 240 sm, the estimates for a particular wavenumber band do not significantly differ with latitude. Comparisons with Eriksen's (1981) displacement spectra require multiplication of these estimates by $N_0^2 \times 10^4$ s cm^2/sm^2 and no significant differences are apparent. Although Hayes (1981) finds significant equatorial enhancement for wavelengths between 306 and 48 sdb, he finds no enhancement for ζ at wavelengths longer than 300 sdb, in substantial agreement with our estimates.

c. Cross-correlation coefficients

Since the vertical scales in the profiles at various latitudes differ (apparent in the autospectra discussed above), a simple measure of intensity of the features evident in the profiles seems warranted. Cross-correlation coefficients calculated between WKB-scaled profiles at different latitudes are presented in Table 1 for the profiles shown in Fig. 3b. Pairs of profiles that span 2°N are negatively correlated with 40–60% of the variance explained by a phase reversal. Similarly, pairs of profiles equatorward of 2°N are positively correlated, at approximately the same level. Note that the least variance is explained when the equatorial profile is compared to profiles more than a degree

TABLE 1. Cross-correlation of zonal velocity profile pairs at various latitudes, using the bottom 3600 sm of each profile. All profiles are from latitudinal section 3, 2–5 June 1976.

Location of profiles (1)	Location of profiles (2)	R_{u_1,u_2}	$R^2_{u_1,u_2}$
	(a) antisymmetry across 2°N		
1°30′N	3°N	−0.77	0.59
0°45′N	3°N	−0.76	0.58
0°	3°N	−0.62	0.38
	(b) symmetry between equator and 2°N		
0°45′N	1°30′N	0.79	0.63
0°	0°45′N	0.74	0.54
0°	1°30′N	0.63	0.40
	(c) symmetry across equator		
0°45′S	0°45′N	0.73	0.53

away, a fact related to the shorter vertical scales present at and near the equator. The last line of the table examines the degree of persistence across the equator, which accounts for 53% of the variance.

d. *Cross-spectra*

Cross-spectra were estimated at each profile station between the three variables, u, v and ζ, and also between the same variable at different latitudes. Statistical stability was obtained by piece-averaging, treating each profile as a separate piece, rather than by wavenumber averaging. Significant coherence amplitude and nonzero phase relationships were found between variables at the same location, but no patterns emerge, either in adjacent latitudes, adjacent wavenumber bands or interpretable relationships between variables in the same band at the same latitude. The exceptions are the cross-spectral estimates for a vertical wavelength of 400 sm at 0°45′N. At the equator coherence is significant between u and v with a phase difference $>\pi/2$. At 0°45′N all three variable pairs are coherent, with u leading v by $\pi/2$, ζ leading u by $\pi/2$, and v and ζ 180° out of phase. The phase differences at 0°45′N are consistent with a mixed Rossby–gravity wave at that vertical wavelength although the coherence at the equator is not. Although the equatorial Rossby radius of deformation, i.e., the e-folding scale for mixed Rossby–gravity waves, is less than ¾° for vertical wavelengths less than 500 sm, the energy in the north velocity component would be 27% of that at the equator for a 400 sm wavelength, while the energy in east velocity would be 46% of that of north velocity at the equator. The theoretical phase relationships are thus resolvable at this latitude for this wavelength.

From linear equatorial wave theory, the only significant coherence expected at the equator is between u and ζ, with a phase relation of $\pm\pi/2$, for odd meridional modes. Eriksen (1981) found such a pattern for wavelengths longer than 200 sdb, with ζ leading u by $\pi/2$, and interpreted it as evidence of Kelvin waves. Hayes (1981) did not find such a pattern, and no such pattern is found in the data discussed here. The only coherence Hayes (1981) found at the equator was between u and v.

The cross-spectrum between zonal velocity profiles at different latitudes agrees with an inspection of the profiles and the cross-correlation coefficients of Table 1. Zonal velocity at the equator is coherent (significant at the 95% confidence level) with all five other profile stations for the longest wavelengths resolvable, 1800 and 1200 sm, with a phase difference indistinguishable from zero at ±0°45′ and 1°30′N. (The sole exception is the lack of coherence at 1200 sm between the equator and 1°30′N.) The phase difference between east velocity at the equator and 3°N is close to π, indistinguishable from π at 5°N for the 1800 sm band; close to π at 3°N and zero at 5°N for the 1200 sm band. East velocity at the equator is not coherent with 5°N at wavelengths shorter than 1000 sm.

There is higher coherence between the equator and 0°45′N than between any other pair of latitudes. Only at a wavelength of 400 sm is the phase difference between the two latitudes nonzero, and there it is only marginally so, i.e., any wavenumber averaging would yield zero-phase estimates. In general, coherence falls off away from the equator with decreasing wavelength, confirming the concentration of energy observed in the autospectra of Fig. 6. The phase differences are either indistinguishable from zero or from π, consistent with meridional modes.

e. *Dropped lagged coherence*

Figure 8 is a superposition, for the zonal velocity component, of the dropped lagged coherences (DLC) for each temporal lag resolvable at the equatorial station at 53°E. The overall pattern is one of high coherence amplitude and zero phase estimates at the longer wavelengths. For the lowest vertical wavenumber bands resolvable, the dropped lagged coherence calculations yield significant coherence: for wavelengths of 1800, 900, and 720 sm, at least seven of the eight resolvable temporal lags at the equator yield coherence estimates significant at the 95% confidence level. At 0°45′N, coherence between the lagged zonal velocity components is also high: significant for ⅔ of the six lags for 1800 sm, ⅚ for 1200 sm, and at all lags for 720 sm. For none of these, however, is the phase estimate significantly different from zero. The energy observed at those vertical wavelengths is not propagating vertically (cf. Fig. 7, Part I).

The only vertical wavelength for which the DLC calculations at the equator yield both sufficiently high

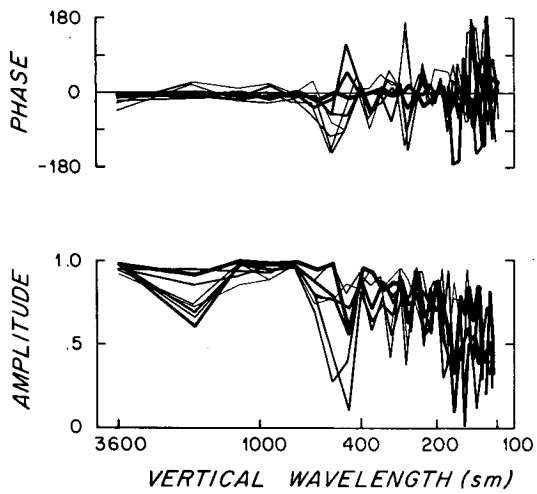

FIG. 8. Superposition of dropped lagged coherence for zonal velocity at 0°, 53°E. All eight resolvable temporal lags are presented, from one day through 19 days. The curves shade from heavy to light with increasing temporal lag.

coherence to be significant and phase estimates which are significantly nonzero is 400 sm. The range of periods which are consistent with the phase change with temporal lag is 105–216 days, with phase propagation upward. At 0°45′N, the 400 sm band is coherent for half the temporal lags examined, and two of the phase estimates are nonzero. However, the phases are uniformly negative indicating phase propagation in the opposite direction (downward) from that at the equator, although encompassing the same period range (47–295 days at 0°45′N).

4. Interpretation and discussion

At present, both the kinematics and the dynamics of these observations are somewhat unclear. As we noted above, there are superficial similarities between these observations and linear equatorial waves. The theory of linear equatorial waves has been developed extensively and reviews on the current status of the theory and its applicability have been published recently (Moore and Philander, 1977; Leetmaa *et al.*, 1981). Linear theory predicts the existence of low frequency equatorially trapped waves at all vertical wavelengths. Meridional scale and zonal wavelength decrease with decreasing vertical scale.

In particular the meridional trapping scale depends upon the equatorial radius of deformation ($L_R = \sqrt{c/\beta}$) and the meridional mode number ($n = -1, 0, 1, \cdots$). Since the separation constant c is inversely proportional to the meridional mode number, the shortest vertical scales will be most closely trapped to the equator. This result is evident in the observed spectra (Fig. 6) and also in the latitudinal sections. The meridional symmetry and phase relations between the velocity components are determined in part by n. Zonal (meridional) velocity components vanish at the equator for even (odd) meridional mode numbers. The dominance of one of these linear modes will result in a simple meridional structure which can be tested against the data.

a. Kelvin waves

If Kelvin waves dominate the zonal velocity field near the equator, the latitudinal distribution of energy will scale with L_R. The theoretical structure with latitude of higher meridional modes is more complex, involving sums of Hermite polynomials modified by a Gaussian. Any test more sophisticated than that for merely Kelvin waves requires assignment of amplitudes and frequencies to higher meridional modes, such as that attempted by Eriksen (1981).

Table 2 contains a comparison of the energy ratios between 0°45′N and the equator to the ratios consistent with a deformation radius scaling, for the averaged vertical wavelength bands centered at 720, 360 and 240 sm, where equatorial intensification appears strongest. The indication from the table is that Kelvin waves are not dominant at these vertical scales. This is consistent with the absence of a significant coherence between zonal velocity and displacement at the equator.

b. Rossby waves

The Rossby waves have more complicated meridional structures with reversals in the phase of zonal velocity at various latitudes. In Section 3c we discussed the meridional structure and found that a reversal in phase occurs between 1°30′N and 3°N with no phase change between 0°45′S, 0° and 0°45′N.

Wunsch (1977) suggested that the observed persistence and meridional structure were consistent with a first meridional mode ($n = 1$) Rossby wave generated near the surface by semiannual components of the wind. There are other reasons to consider a semiannual period. Although no information on periodicity was obtained from these data at long vertical scales, using the only method available (DLC), the strongest signal in the ~400-day series of current meter measurements from the western equatorial Indian Ocean

TABLE 2. Equatorial trapping of zonal velocity.

		Autospectral estimates [(scm/s)²/cpsm]		Energy ratios	
λ_z^* (sm)	L_R (km)	0°	¾°N	est ¾°N / est 0°	$e^{-(¾°N/L_R)^2}$
720	98	238 (180–340)†	236 (179–339)	0.99	0.48
360	69	36 (28–50)	33 (25–46)	0.92	0.24
240	56	19 (14.5–26)	15.5 (12–22)	0.82	0.12

† Parentheses indicate 95% confidence limits.

TABLE 3. Theoretical structure of gravest odd meridional mode long Rossby waves of 180-day period.

		1500 sm			λ_z^* Mode	1800 sm
	Latitude	1	3	5		1
λ_x (km)		−2253	−886	−502		−2726
East velocity structure						
Nodes (km [°])		±171 [±1°33′]	86, 301	67, 210, 397		±187 [±1°45′]
	0°45′	0.65	0.07	−0.33		0.70
Amplitude decay with latitude	1°30′	0.03	−0.93	−0.79		0.13
(as fraction of equatorial	3°	−0.18	0.18	0.68		−0.21
amplitude)	5°	−0.00	0.05	−0.17		−0.01
Off-equatorial maxima, km [°]		±262 [2°23′]	177, 382	136, 228, 473		±288 [2°37′]

in 1979–80 is for a 180-day period oscillation in east velocity (Luyten and Roemmich, 1982). Knox (1976) and McPhaden (1982) also show strong semiannual variability at Gan Island. Note that increasing the period beyond the semiannual would increase the zonal wavelength, according to linear theory, but would have little effect upon the latitudinal structure of the zonal velocity field.

Table 3 gives some of the possible consistency checks between the data and a first meridional mode long Rossby wave of semiannual period. The primary points for comparison are the zonal scale of the phenomenon, the latitudes where a 180° phase reversal occurs, and the relative amplitudes at various latitudes.

The zonal scale cannot be resolved from the 1976 data: Figure 9 shows pairs of near-simultaneous profiles from the two equatorial stations, at 50°30′E and 53°E. Two weeks elapsed between each pair, and there are no clear phase differences with longitude or with time. The former indicates that the zonal scale is much longer that the separation between the stations (275 km) and the latter is consistent with a period, if any, of at least six months, i.e., six times the elapsed time between the first and last of the profiles at each station.

The second point of comparison is the latitude of phase reversal, which in the data occurs somewhere between the stations at 1°30′N and 3°N. An estimate of 1500 sm for the vertical wavelength gives a phase reversal just to the north of the first station, while an estimate of 1800 sm pushes that location 17 km further towards 2°N.

The third point of comparison is the amplitude decay of the zonal velocity associated with a first-mode Rossby wave from its primary maximum at the equator. Table 3 indicates that this is where the major discrepancy in such an interpretation arises. Amplitudes at the equator and ±0°45′ would be comparable, as would amplitudes at ±1°30′ and ±3°, for a vertical wavelength of 1800 sm. The data do not indicate the decrease in relative amplitude between these pairs of latitudes, however. An 80% decrease in amplitude between the equator and 3°N would incline one to the view that a feature observable at the equator would not be manifest at 3°N.

It thus seems unlikely that the antisymmetry across 2°N is due solely to the presence of a linear first meridional mode Rossby wave. Higher odd meridional-mode Rossby waves might be responsible but are rejected because a node in the zonal velocity field would be expected between 0°45′N and 1°30′N (or closer to the equator), although the relative amplitudes might remain higher in that case, as in Table 3.

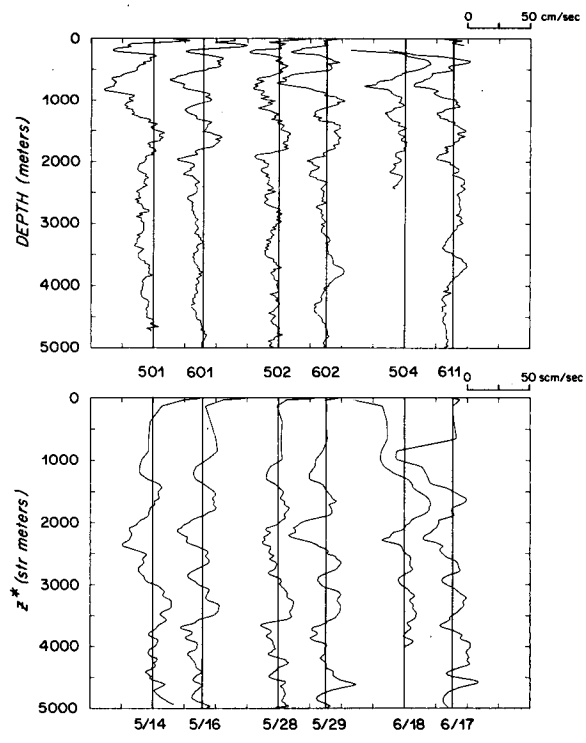

FIG. 9. Comparison of pairs of zonal velocity profiles at the equator. The first of each pair is from 0°, 50°30′E; the second from 0°, 53°E. Each pair was separated by approximately two weeks from the adjacent pair(s). (a) Unscaled data; (b) WKB-scaled data.

As we said above, more complicated meridional structures can be obtained by summing the modes. In fact, any shape which is meridionally bounded can be reproduced. Such a calculation requires assigning amplitudes and phases to the various modes, for which there is little *a priori* justification.

c. *Something else*

The Indian Ocean is not bounded by simple meridional walls and has intense and highly variable currents. The meridional structure of simple linear equatorial waves may be disrupted near slanting meridional boundaries, such as the Somali Coast. Far from the meridional boundaries, the modes will look like those calculated for straight meridional boundaries (Cane and Gent, 1984). In the far field the amplitude and phase of the gravest (vertical) symmetric modes show little change due to the slanting coast, although the antisymmetric and higher (vertical) symmetric modes show greater differences. Exactly how far from the boundary one needs to be in order to be in the far field is not clear. When these observations were planned, it was felt that 53°E was far enough; this assumption may not be correct. To date, no solutions have been published for the near-field problem. It seems clear that in the near field, the simple phase relations between the velocity components, characteristic of free equatorial waves, must be altered. Further theoretical work is needed before we can address these effects in our data.

5. Conclusions

The observations discussed here were the first to demonstrate the existence of small vertical scale structures in the equatorial zonal velocity field which are coherent in time (~ one month) and latitude (several degrees). In broad outline, these observations of long period fluctuations with vertical scales of several hundred to a thousand meters are consistent with equatorially trapped motions. The smaller vertical scales are more tightly trapped, and the 1200–1500 stretched meter feature extends coherently from the equator to 3°N, where it is out of phase with the equator. This is similar to what would be expected from a first meridional-mode Rossby wave. The absence of coherence phases other than 0° and 180° suggests a (standing) meridional mode. However, the linear theory predicts a meridional shape of these modes which decays and/or oscillates much more rapidly than our observations indicate. This is also true for the shorter vertical scale motions near the equator. For these shorter scale motions, we may be confident that they are symmetric about the equator (0°45′S and 0°45′N are coherent with the equator at zero phase). We cannot be so confident for the larger vertical scale features which extend further, coherently, to the north than our observations extend to the south. As we have noted in the previous section, these vertical scales are likely to be affected by the sloping boundary of the Somali coast.

For the longer vertical scales, there are no significant variations over the observation period of one month. For the 400 sm structure, the dropped lagged coherences suggest vertical phase propagation with a period in the range 4 ± 3 months, although the equator shows upward phase propagation whereas at 0°45′N propagation is downward. There is no consistent evidence for vertical propagation.

Neither of these results is particularly edifying. We are forced to conclude that, although the observations indicate equatorially trapped long-period motions with vertical scales small compared to the ocean depth, these phenomena are not consistent with the kinematics of free linear equatorial waves in the absence of meridional boundaries and mean currents. In the absence of vertical propagation, it is quite difficult to rationalize their existence in the deep ocean. It is true that at present no theory exists for linear waves in the near field of a strongly sloping boundary. That appears to be the only hope at this point for rescuing a simple interpretation in terms of linear theory.

Acknowledgments. We wish to thank the National Science Foundation for their generous support under Grants ATM 76/2196 and ATM 78/21491 during the field and analysis phases of this work.

REFERENCES

Cane, M. A., and P. R. Gent, 1984: Reflections of low-frequency equatorial waves at arbitrary western boundaries. *J. Mar. Res.*, **42**, 487–502.

Cochrane, J. D., F. J. Kelly, Jr. and C. R. Olling, 1979: Subthermocline currents in the western equatorial Atlantic Ocean. *J. Phys. Oceanogr.*, **9**, 724–738.

Eriksen, C. C., 1981: Deep currents and their interpretation as equatorial waves in the western Pacific Ocean. *J. Phys. Oceanogr.*, **11**, 48–70.

Hayes, S. P., 1981: Vertical fine structure observations in the eastern equatorial Pacific. *J. Geophys. Res.*, **86**, 10983–10999.

Hisard, P., J. Merle and B. Voituriez, 1970: The Equatorial Undercurrent at 170°E in March and April 1967. *J. Mar. Res.*, **28**, 281–303.

Knox, R. A., 1976: On a long series of measurements of Indian Ocean equatorial currents near Addu Atoll. *Deep-Sea Res.*, **23**, 211–222.

Kort, V. G., B. A. Burkov and K. A. Chekotillo, 1966: New data on equatorial currents in the western Pacific. *Dokl. Akad. Nauk. SSSR*, **171**, 337–339 (in Russian).

Leetmaa, A., J. P. McCreary, Jr. and D. W. Moore, 1981: Equatorial currents: Observations and theory. *Evolution of Physical Oceanography*, The MIT Press, 184–197.

Levy, E., A. Spencer, G. Needell, G. Hund and J. R. Luyten, 1982: A compilation of moored current meter data, White Horse profiles and associated oceanographic observations, Volume XXIX (INDEX, 1979), WHOI Ref. No. 82–11, 39 pp.

Luyten, J. R., 1982: Equatorial current measurements, I: Moored observations. *J. Mar. Res.*, **40**, 19–41.

——, and J. C. Swallow, 1976: Equatorial undercurrents. *Deep-Sea Res.*, **23**, 1005–1007.

——, and D. H. Roemmich, 1982: Equatorial currents at semi-

annual period in the Indian Ocean. *J. Phys. Oceanogr.*, **12**, 406–413.

McPhaden, M. J., 1982: Variability in the central equatorial Indian Ocean, Part I: Ocean dynamics. *J. Mar. Res.*, **40**, 157–176.

Molinari, R. L., 1982: Observations of eastward currents in the tropical South Atlantic Ocean: 1978–1980. *J. Geophys. Res.*, **87**, 9707–9714.

Moore, D. W., and S. G. H. Philander, 1977: Modeling of the tropical ocean circulation. *The Sea*, Vol. 6, E. D. Goldberg, I. N. Cave, J. J. O'Brien and J. M. Steek, Eds., Interscience, 319–361.

O'Neill, K., 1982: Observations of vertically propagating equatorially-trapped waves in the deep western Indian Ocean. Ph.D. dissertation, The Johns Hopkins University, 161 pp, [also W.H.O.I., Tech. Rep., 82-11].

——, 1984: Equatorial velocity profiles. Part I: Meridional component, *J. Phys. Oceanogr.*, **14**, 1829–1841.

Rual, P., 1969: Courants équatoriaux profonds. *Deep-Sea Res.*, **16**, 387–391 (in French).

Sanford, T. B., 1975: Observations of the vertical structure of internal waves. *J. Geophys. Res.*, **80**, 3861–3871.

Spencer, A., K. O'Neill and J. R. Luyten, 1980: A compilation of moored current meter data, White Horse profiles and associated oceanographic observations, Vol. XXIV (Indian Ocean array, 1976). WHOI Ref. No. 80-41, 46 pp.

Taft, B. A., B. M. Hickey, C. Wunsch and D. J. Baker, Jr., 1974: Equatorial Undercurrent and deeper flows in the central Pacific. *Deep-Sea Res.*, **21**, 403–430.

Tsuchiya, M., 1975: Subsurface counter currents in the eastern equatorial Pacific Ocean. *J. Mar. Res.*, **33**, 145–175.

Weisberg, R. H., and A. M. Horigan, 1981: Low-frequency variability in the equatorial Atlantic. *J. Phys. Oceanogr.*, **11**, 913–920.

Wunsch, C., 1977: Response of an equatorial ocean to a periodic monsoon. *J. Phys. Oceanogr.*, **7**, 497–511.